CrossMark

Thermal aging effects on microstructure, elastic property and damping characteristic of a eutectic Sn–3.5Ag solder

Asit Kumar Gain[1] · Liangchi Zhang[1]

Abstract

The present work describes the microstructural changes and their impacts on the electrical resistivity, elastic modulus and damping property of a eutectic Sn–3.5wt% Ag solder material when exposed to high temperature. A detail microstructural study was conducted through the scanning electron microscopy with energy-dispersive spectroscopy analysis and electron backscattered diffraction technique. In as-cast eutectic Sn–Ag solder alloy, sub-micrometer size Ag_3Sn intermetallic compound (IMC) particles and bamboo-like dendritic structure with a dimension of length 20–30 μm and width 3–5 μm formed during solidification. However, after thermal aging treatment at 150 °C for 60 days, the fine Ag_3Sn IMC particles and β-Sn grain appeared with coarse microstructure with the formation of twinning having the <100> twin axis and 60° rotation. As a result, microstructure and Sn-crystal orientation of Sn–Ag solder greatly impact on its overall properties and turned inferior. From material properties evaluation, it was confirmed that the electrical resistivity, elastic and shear moduli values were significantly reduced with aging time. Consequently, the values of damping capacity improved due to the reduction of moduli.

1 Introduction

Continuous pursuit of portability and miniaturization in the evolution of electronic components and devices towards higher packing density shrinks the dimensions of the electronic interconnections [1]. As a result, the current density across the electronic interconnections was increased significantly which leads to a serious reliability problem at high level current-stressing. Accordingly, the necessity for high integrity and mechanical reliability become a critical challenge in the electronic interconnection performances particularly under the harsh service environments [2, 3]. Generally, lead-containing (Sn–37Pb) solder was broadly used in microelectronic devices to assemble the electronic components to the printed circuit boards (PCBs) because of its outstanding mechanical properties, well-known process attributes as well as low cost [3–5]. Nowadays, however, the

application of lead-based alloys in microelectronic packaging industries is restricted due to their toxicity to human health and environment [5–7]. Therefore, for more than three decades, significant researches have been placed on development and manufacturing of a lead-free Sn-based interconnect material for green electronic devices [8–13]. Among the new generation environmental-friendly Sn-based electronic interconnect materials, the near eutectic or eutectic Sn–Ag based solders are considered as an appropriate candidate materials to replace the lead containing solders in electronic packaging industries [14–17]. Sn–Ag solder alloy possess several fascinating features such as good wettability on widely used substrates such as Cu and Ni, good strength, superior drop reliability and better resistance to thermal fatigue and creep [16–18]. Furthermore, Sn–3.5Ag solder alloy has a eutectic point at 221 °C and contains a homogeneous distribution of Ag_3Sn IMC particles which significantly influence the mechanical reliability [18]. However, during the service environments, the device typically experiences temperature fluctuations, strain/stress cycle and mechanical or vibration shock with changing the environments or self-generated heating in response to switch on and off the devices [19–21] which may gradually change the microstructure and electrical/mechanical performance of electronic interconnections. Furthermore, the advanced microelectronic devices are commonly used in different

✉ Asit Kumar Gain
a.gain@unsw.edu.au

Liangchi Zhang
liangchi.zhang@unsw.edu.au

[1] Laboratory for Precision and Nano Processing Technologies, School of Mechanical and Manufacturing Engineering, University of New South Wales, Sydney, NSW 2052, Australia

vibration forms and various level of acceleration, which may damage of the electronic interconnections and initiate the failure of electronic products [22, 23]. Thus, it is essential to recognize the capacity of interconnect materials to dissipate energy through vibration that denotes the damping property. To the best of our literature review and knowledge, only few efforts has been done to figure the damping properties of as-cast lead-containing and lead-free Sn-based solder materials [23–27]. However, it is indeed very important to estimate the damping properties of Sn–3.5Ag solder material when subjected to harsh service environments. In general, the reliability study (e.g., under bump metallization (UBM), the physical and mechanical properties of IMC layer and strength) of electronic interconnections are carried out after isothermally aging (at 150 °C) with changing aging time (250–1500 h) [28, 29]. These conditions are frequently used in two main reasons; firstly IMC growth facilitated at this environment [29, 30] and secondly industrially this environment is accepted for simulating the harsh operating condition. The objective of this work is therefore to explore the changing of microstructure, electrical resistivity performance, elastic moduli and damping capacity of Sn–3.5Ag material after exposed to the harsh service conditions (i.e., isothermally aged at 150 °C). Further, focusing to measure their temperature-dependence and strain amplitude-dependence damping property at various operating temperatures.

2 Experimental procedures

2.1 Materials and microstructure characterization

Commercially available environmental-friendly as-cast eutectic Sn–3.5Ag solder material (purity 99.8%, Shenzhen Jufeng Solder Company LTD., China) were cut into cuboid pieces with a dimension of about $40.0 \times 7 \times 2.2$ (in mm) through wire cutting process. During this process cosmos machinery coolant (Dx-1) is used to minimize the heat generation. After that the cutting specimens were grounded by various grit sizes SiC papers and then polished by Al_2O_3 suspension with a dimensions of about $40.0 \times 6.8 \times 1.8$ (in mm). Then one set of samples was placed at high temperature chamber with a constant temperature of 150 °C. Then their microstructures were analysed by metallography technique. The polished specimens were etched for 10–15 s in the solution which contained C_2H_5OH (99 vol%) and HCl (1 vol%) to observe the microstructure of Sn–3.5Ag solder. Finally, microstructure and IMC composition were examined through scanning electron microscopy (SEM, Hitachi S3400) and EDS analysis. Further, to obtain the crystallographic information electron backscattered diffraction (EBSD) (Carl Zeiss Auriga, FEG) was used. Then the EBSD data was analyzed through Channel 5™ software.

Before analyzing the specimens through EBSD technique, the mechanically polished specimens were milled through an ion milling machine (Hitachi IM4000) with a wide angle of 3.5 kV ion beam. Crystalline structure of both as-cast and aged specimens was studied using X-ray diffraction (X'pert Pro MPD) technique. This system is typically configured with a copper source, providing X-rays with a wavelength of 1.54 Å.

2.2 Property measurements

2.2.1 Damping capacity

Temperature-dependence and strain amplitude-dependence damping properties were measured by a dynamic mechanical analyzer (DMA, TA 2980) of as-cast and thermal aging at 150 °C for 60 days. The single-cantilever mode was used during the damping capacity measurement.

2.2.2 Modulus measurement

Elastic properties such as elastic and shear moduli were evaluated using IMCE equipment (RFDA HT 1050) at room temperature following an impulse excitation method. Ten such impact tests were carried out on each specimen a dimension of $40.0 \times 6.8 \times 1.8$ (in mm) for obtaining an acceptable average data. Briefly on this technique, the specimen is suspended using metal wire in a chamber and impacted through a ceramic rod. During impaction of the specimen, the emitted torsion and flexural vibration signals were captured through a microphone and analyzed by Fast Fourier Transform [31].

2.2.3 Electrical resistivity measurement

Electrical resistivity at different operating temperatures (i.e., in a range of room temperature to 100 °C) was conducted by an Agilent E4980A precision LCR meter. For each condition three samples were used for obtaining an acceptable average data.

3 Results and discussion

Figure 1 illustrates the SEM images of Sn–3.5Ag material depending on isothermal aging period; (a, b) as-cast, (c, d) 20 days aging and (e, f) 60 days aging. Through SEM characterization, it was confirmed that sub-micrometer sized Ag_3Sn IMC phase was generated with network-type structure in β-Sn matrix during the solidification. Laurila et al. described in detail through the phase diagram and mentioned that two intermetallic compounds grew during the solidification process of Sn–Ag alloy. One of them is the
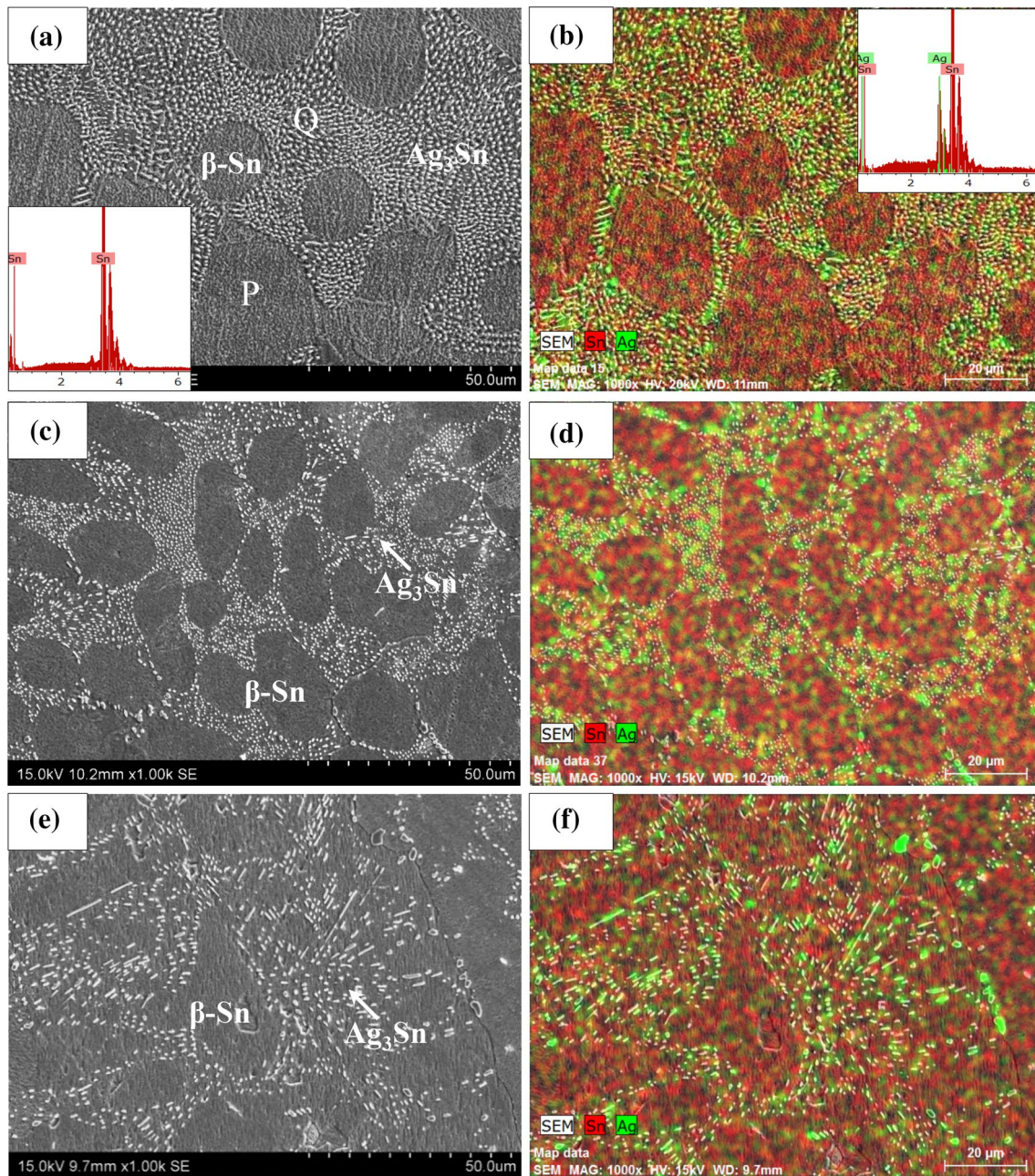
Fig. 1 SEM images and elemental mapping of Sn–3.5Ag solder at various aging periods; **a**, **b** as-cast, **c**, **d** 20 days and **e**, **f** 60 days

disordered cph phase ζ and the other is the orthorhombic short-range ordered Ag_3Sn (ε) [32]. In the as-cast materials as shown in Fig. 1a, b, a spheroidal or quasi-sphere ε-Ag_3Sn IMC particles were dispersed in Sn-rich dendritic matrix. However, after thermal treatment this IMC particle size was changed and appeared with both plate-like and spheroid-like IMC particles as shown in Fig. 1c–f. The formation of large Ag_3Sn plate can adversely affect the plastic deformation of Sn–Ag alloy [33]. Henderson et al. also reported three phenomena related to the grain boundary sliding e.g., (i) strain

localization and large strains due to grain boundary sliding at the interface of Ag_3Sn plates and the β-Sn matrix; (ii) preferred crack initiate at the interface of plate-like ε-Ag_3Sn and the β-Sn matrix, (iii) localization of large strains within the β-Sn matrix at the terminus of ε-Ag_3Sn plates [34]. Figure 1b, d, f present the elemental mapping corresponding to the SEM image of Fig. 1a, c, e. From elemental mapping analysis, it was found that the needle-shape IMC particles consist of Ag and Sn elements whereas the dark contrast matrix appeared with Sn element. Further, EDS analysis was

carried out as marked "P" and "Q" regions in Fig. 1a. The inserted EDS profile at bottom corner as marked "P" region as seen in Fig. 1a presented that the dark contrast matrix appeared with Sn element whereas marked "Q" region the needle-shape IMC particles consisted Ag and Sn elements as seen EDS profile inserted at top corner in Fig. 1b.

Figure 2 illustrates the XRD pattern of Sn–3.5Ag solder material; (a) as-cast condition and (b) the sample aged for 60 days at 150 °C. From this investigation, it was noted that Ag_3Sn IMC phase was appeared in the β-Sn matrix phase. It is understandable that Sn and Ag elements dissolved during processing and grew Ag_3Sn IMC particle in the β-Sn matrix subsequent solidification process. However, after isothermal aging seen in Fig. 2b, no additional crystalline phase was detected. Therefore, the XRD result confirmed that the isothermal aging treatment of as-cast Sn–Ag solder alloy did not grow any other crystalline IMC phase.

To understand the crystallographic information's for example grain size and orientation, large area EBSD scan was carried out in the as-cast Sn–Ag solder material. Unique grain color mapping are presented in the relevant micrographs in Fig. 3a–e. Grains are separated in different colors with a misorientation angle higher than 15°. In EBSD low magnification transvers surface image as shown in Fig. 3a, b, the network type Ag_3Sn IMC phase was found in β-Sn matrix as evidenced in inserted phase image. However, in certain direction dendrite-shape Sn phase was grown in different orientation as marked in dotted rectangular box in Fig. 1a. To clearly observe the dendrite structure the specimen was cross-sectioned by a wide angle 3.5 kV ion beam (Hitachi IM4000). In cross-sectioned EBSD image as shown in Fig. 3c, in low magnification image unidirectional columnar structure was originated. However, in inserted phase map
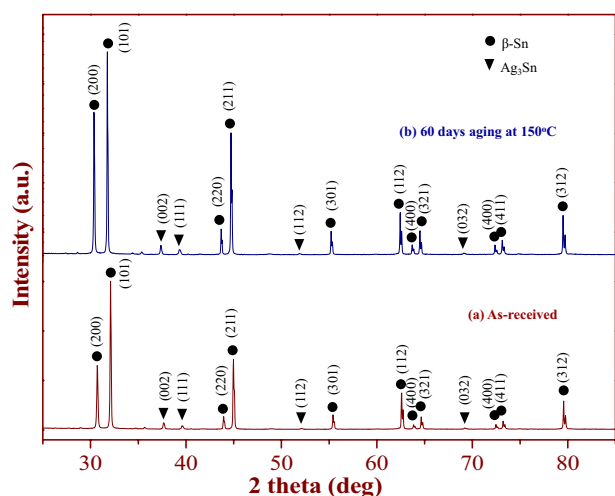
image (see in Fig. 3d) the fine Ag_3Sn IMC network structure was observed in β-Sn matrix. Further in the enlarge image (Fig. 3d, e) fine bamboo-like Sn dendrite structure (e.g., length 20–30 μm and width 3–5 μm) was found with a special orientation <100> 60° relationship with the matrix grains.

Figure 4 shows EBSD micrographs of Sn–3.5Ag material after exposing at 150 °C for 60 days; (a) transvers surface, (b) high resolution image in eutectic region and (c) and (d) cross-sectional images. In low magnification transvers section EBSD image, the Ag_3Sn IMC particles were observed to be evenly distributed in the eutectic colony that clearly indicated in inserted phase map image (Fig. 4a). However, to understand size of Ag_3Sn particles and Sn grain orientation, the high magnification EBSD image was taken in the eutectic region as shown in Fig. 4b. From this characterization it was noticed that the relatively coarse Ag_3Sn IMC particles (about 1–5 μm) are scattered in different orientation Sn grains. In the cross-section EBSD images (Fig. 4c, d), the eutectic colony and Sn matrix were clearly observed without bamboo-like dendritic structure. The plausible explanation for nonappearance the bamboo-like dendritic structure is due to crystal growth during high temperature aging. However, after isothermally aged specimen, interestingly line-type fine features are generated in the Sn matrix (marked by arrowheads in Fig. 4d). Namely, the line-type fine features detected in the isothermally aged alloy contains cyclic twin boundaries with a special orientation <100> 60° relationship with the matrix grains. In earlier studies, similar results obtained from the EBSD investigation when the eutectic Sn–Ag solder materials cooled with different cooling rate during reflow process. It was reported that the fine feature observed in fast-cooled Sn–Ag solder materials is attributed to the twin boundary with a relationship of <100> twin axis and 60° rotation [35, 36]. This coarsening nature of grains and twin formation during real-life application affects the mechanical reliability of electronic interconnects in modern electronic products that can lead to electronic product failure. Further, Anderson et al. [37] found that coarse primary β-Sn dendritic structure in lead-free solder system degraded the thermal–mechanical fatigue resistance.

In modern miniaturized electronic device, the sizes of electronic interconnections shrink remarkably. Consequently, the current density across the electronic interconnections is increased drastically. Therefore, it is important to measure the electrical property (e.g., electrical resistivity) of a solder material for understanding the overall performance of an advanced green electronic product. Figure 5a illustrates the electrical resistivity of as-cast Sn–Ag material and material exposed at 150 °C with varying the isothermal aged duration—measured at (a) room temperature and (b) different operating temperatures. Electrical resistivity of Sn–3.5Ag solder material decreases gradually from
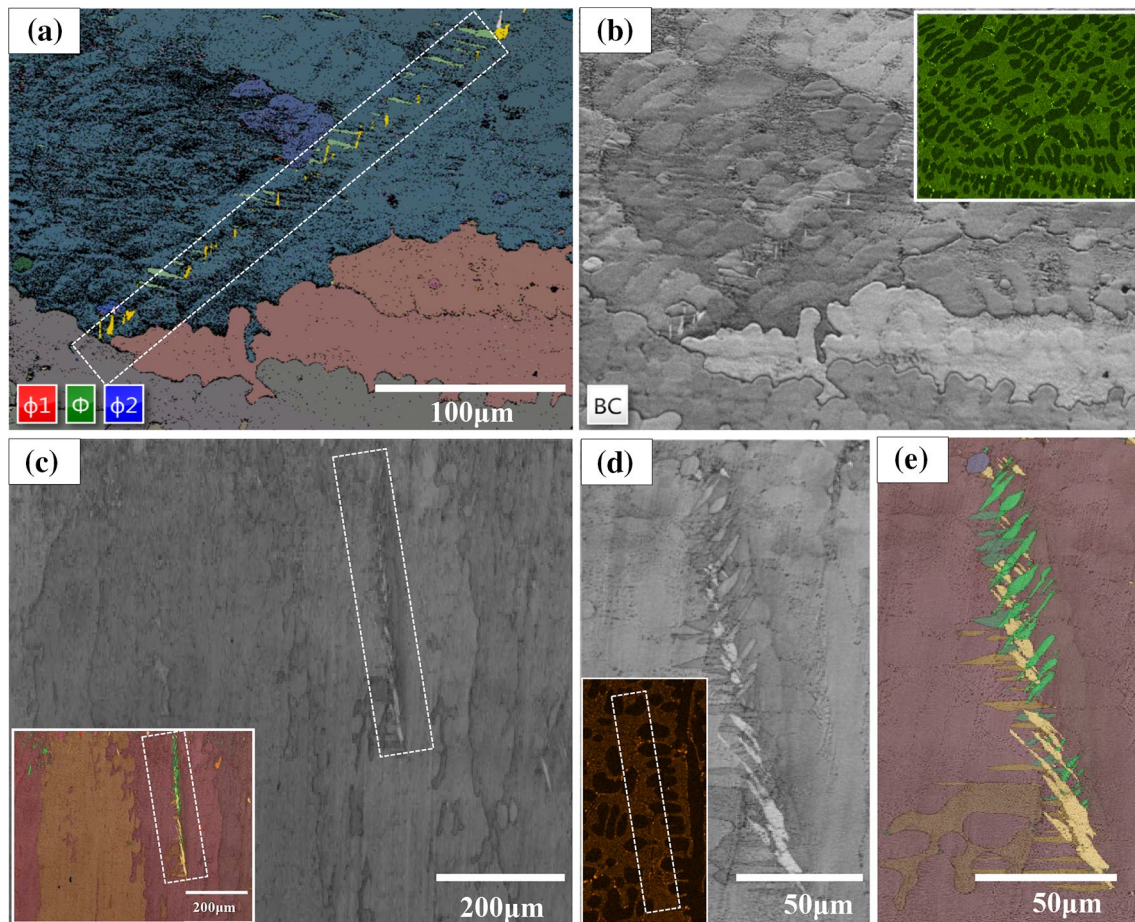

Fig. 2 XRD profiles of Sn–3.5Ag solder material depending on aging time; **a** as-cast solder material and **b** solder material exposed for 60 days at 150 °C

Fig. 3 EBSD micrographs of as-cast Sn–3.5Ag solder material; **a**, **b** transvers surface, **c** cross-sectional and **d**, **e** high resolution images as dendritic structure

12.13 to 10.58 µΩ cm as the isothermal aging period reach to 60 days. The room temperature resistivity value of as-cast Sn–Ag material is similar to the other existing research results. For instance, the resistivity value of environmental-friendly as-received eutectic Sn–0.7Cu and Sn–3.5Ag materials were about 11.93 and 12.0 µΩ cm, respectively [30, 38, 39]. Furthermore, in the temperature dependence measurement it was clear that the electrical resistivity values of both samples were gradually increased with the operating temperatures as presented in Fig. 5b. However, the thermal aged solder material displayed lower resistivity than that of the as-cast solder material. The plausible explanation for indication a lower resistivity is probably to alter the shape, size and uniformity of the IMC phase.

Elastic and shear modulus of environmental-friendly as-cast Sn–3.5Ag solder material and material after exposing at 150 °C for 60 days were measured by the IMCE machine as shown in Fig. 6a. From this measurement, it was confirmed that after exposing at high temperature the elastic and shear moduli values were reduced significantly. The main reason for the degradation of material properties was that the harsh environments influenced the formation of Ag_3Sn IMC phase (size and orientation) as well as increased the β-Sn matrix grains size. The degradation of material properties may negatively impact on the life-span of electronic devices. Figure 6b shows the temperature-dependence damping capacity of as-cast solder material and solder material expose at 150 °C for 60 days—measured at 1 Hz frequency using DMA equipment. The damping property is obtained from calculating the ratio of the loss-modulus to storage-modulus [19]. The damping property increases with the operating temperature. The damping property of as-cast and after exposing to high temperature at 150 °C, the eutectic Sn–Ag solder alloy exhibited a similar pattern. However, the damping property of Sn–Ag solder sample exposed at 150 °C for 60 days appeared to have higher values than that of as-cast sample. From the temperature-dependence damping capacity curve, the values of damping capacity were very low at low temperature (from −100 to −60 °C) of all samples, and then these values increased significantly with temperature. Consequently, the temperature dependence of
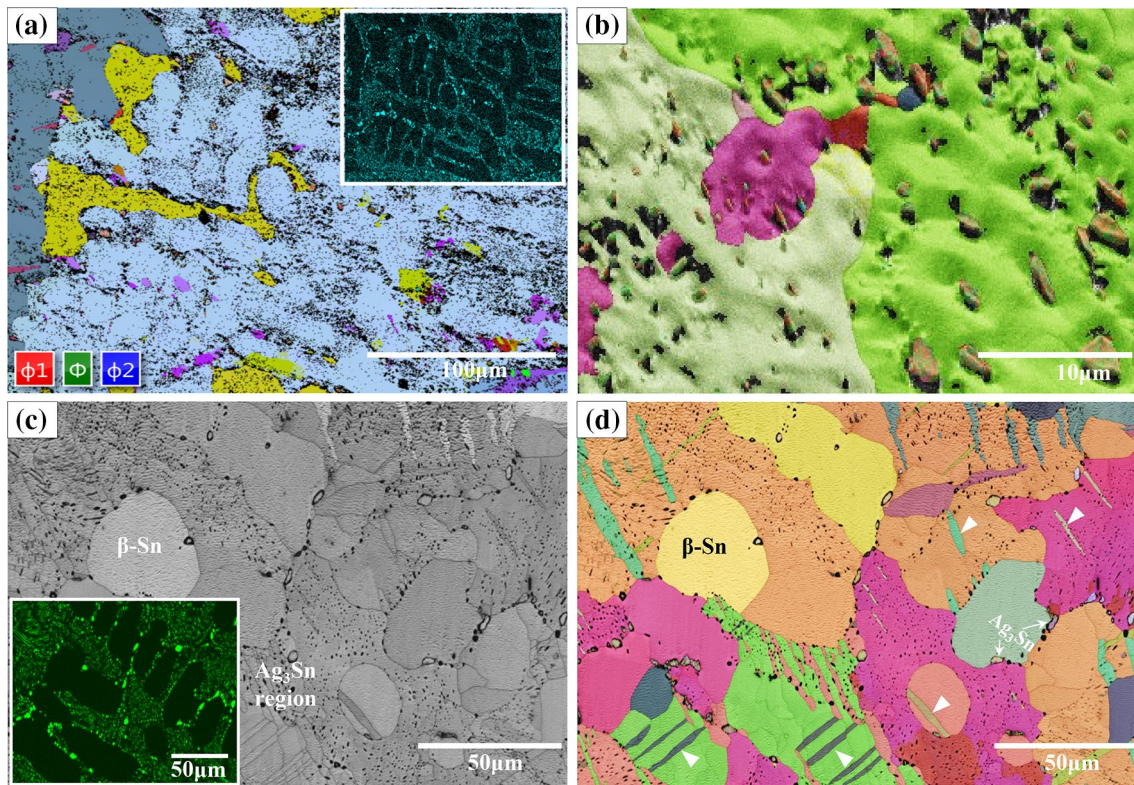
Fig. 4 EBSD micrographs of Sn–3.5Ag material after exposing at 150 °C for 60 days; **a** transvers surface, **b** high resolution image in eutectic region and **c**, **d** cross-sectional images
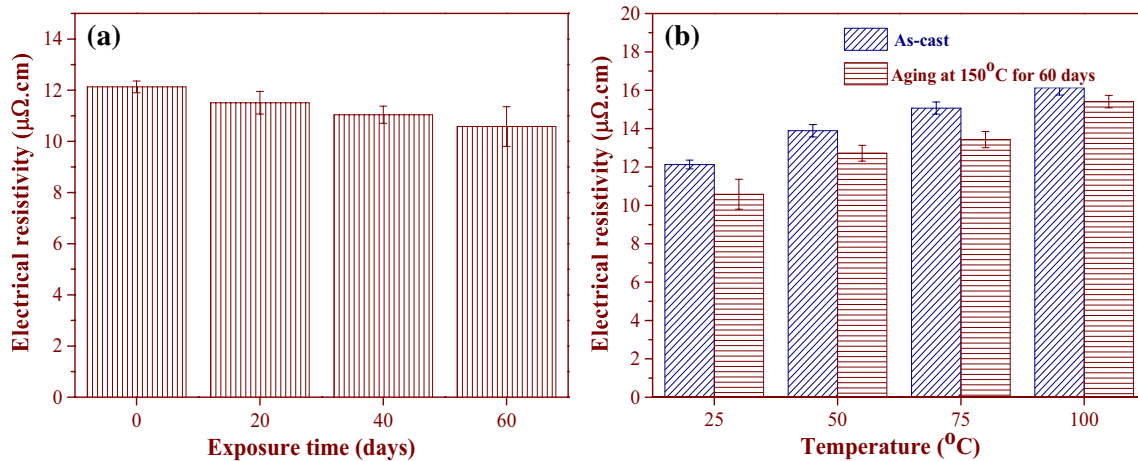

Fig. 5 Electrical resistivity of Sn–3.5Ag material; **a** measured at room temperature relying on aging durations and **b** measured at different operating temperatures of as-cast material and after 60 days aging

damping capacities can be separated into two sections; (i) an ADB (athermal damping background) occurred at low temperature between −100 and −60 °C and (ii) a HTDB (high-temperature damping background) or an exponential damping background achieved at a higher temperature above −60 °C [26, 40]. Similar damping behavior was found in the conventional Sn–37Pb solder alloys [24, 26]. It was clearly stated that the ADB creates through dislocation damping that confirmed by the Granato–Lucke dislocation theory [41]. The temperature dependence damping capacity of as-cast Sn–3.5Ag solder material and solder material expose at 150 °C for 60 days for −100 °C were
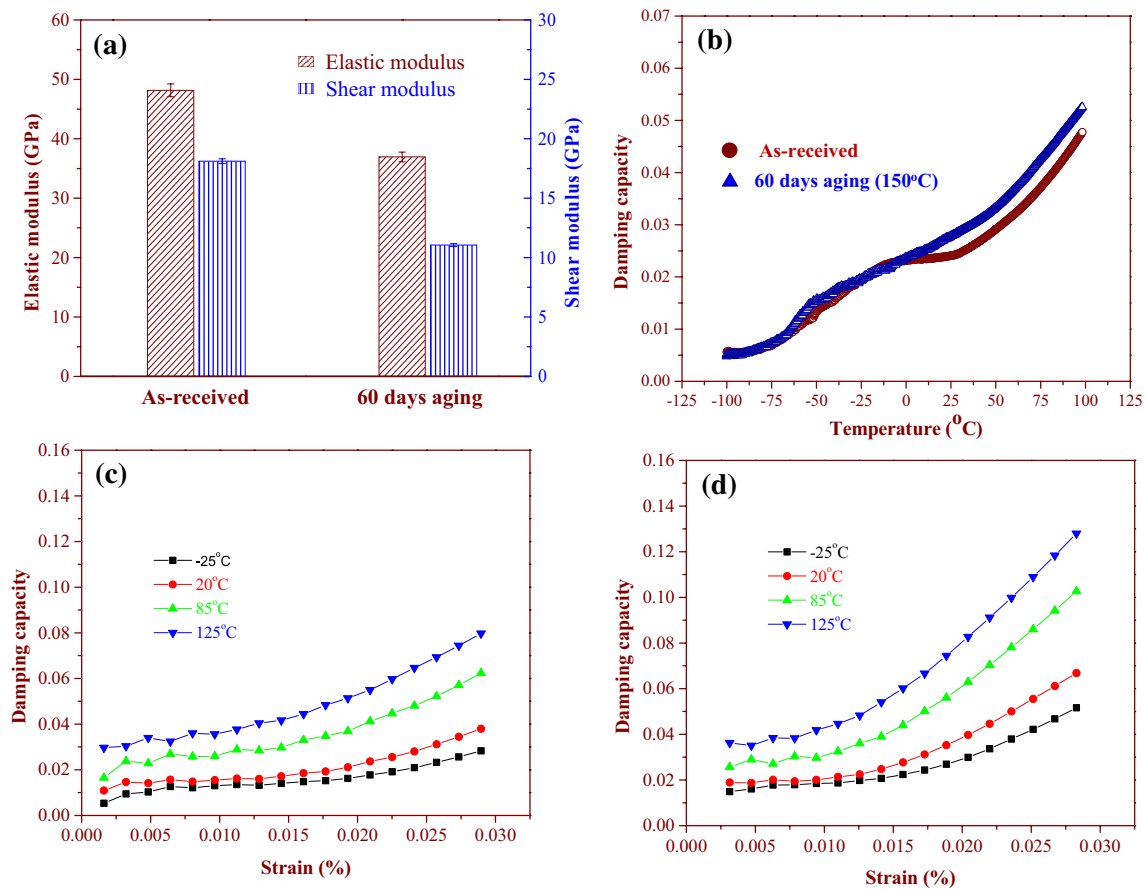
Fig. 6 **a** Elastic and shear moduli, **b** temperature-dependence damping property and **c**, **d** strain amplitude-dependence damping property of Sn–3.5Ag solder material; e.g., **c** as-cast, **d** after aging for 60 days—measured at 1 Hz frequency

about 0.0057 and 0.0062, respectively—while the corresponding values at 100 °C were about 0.048 and 0.053. Figure 6c, d shows the strain amplitude-dependence damping property of eutectic Sn–3.5Ag material after exposure in harsh environments e.g., (c) as-cast and (d) after aging for 60 days—measured at 1 Hz frequency at different operating temperatures in between − 25 °C to 125 °C (homologous temperatures (T/T_m) from 0.5 to 0.8). From this strain amplitude-dependence measurement, the value of damping capacity for as-received alloy measured at − 25 °C ($T = 0.5T_m$) was very low (less than 0.01) at low strain rate and then this value was gradually increase with the strain rate. However, after exposing at harsh environments for 60 days the damping capacities presented slightly higher values (above 0.015) at low strain rate. Moreover, the strain amplitude-dependence damping capacity values also increased with increasing the homologous temperatures (T/T_m) from 0.5 to 0.8. The interesting phenomena were observed after exposing at harsh environments that the values of damping capacities were increased gradually at a range of strain from 0.0025 to 0.015 and then these values were increased significantly. Trojanova et al. [42]

demonstrated that the strain amplitude-dependence damping property presented two main reasons. The damping can be separated by two components;

$$Q^{-1}(\varepsilon) = Q_0^{-1} + Q_H^{-1}(\varepsilon) \tag{1}$$

where Q_0^{-1} is the damping capacity independent/weekly dependent on strain and the damping capacity $Q_H^{(-1)}(\varepsilon)$ is strongly relied on the strain-amplitude. From this investigation, it was found that the damping property of Sn–3.5Ag solder material was primarily dominated by $Q_H^{(-1)}(\varepsilon)$ rather than the Q_0^{-1}. This phenomenon was much obvious in the thermal aging specimens. The damping properties of as-cast Sn–3.5Ag material and solder material aged for 60 days, at low strain for 125 °C, were approximately 0.035 and 0.036, respectively. On the other hand, at high strain their corresponding values were approximately 0.08 and 0.128, respectively.

Figure 7 illustrates the stress versus strain graphs of environmental-friendly Sn–3.5Ag solder material after exposure in harsh environment e.g., (a) as-cast alloy and (b) alloy exposed at 150 °C for 60 days—measured at 1 Hz frequency and different temperatures (from − 25 °C to 125 °C). From
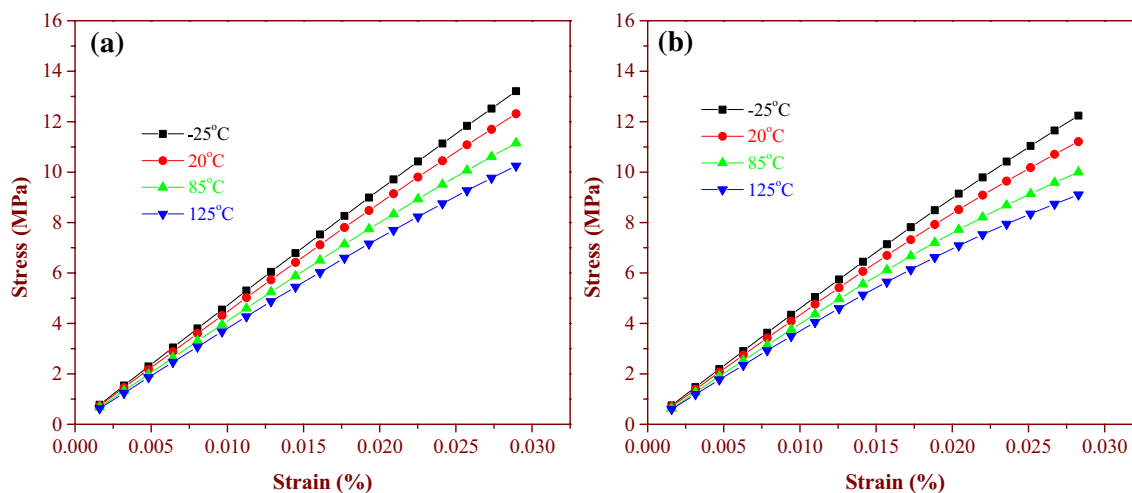
Fig. 7 Stress and strain graphs of Sn–3.5Ag solder material; **a** as-cast and **b** after aging for 60 days—measured at 1 Hz frequency

this stress and strain graphs, the stress of all solder alloys increased linearly with strain value. However, it is worthy noted that the stress values were reduced significantly with their operating temperature. Furthermore, after exposure in harsh environments the stress and strain curves shifted to downward as compared to as-cast Sn–3.5Ag solder material. This feature indicates that the experimental results confirmed indicates that thermal aging of environmental-friendly eutectic Sn–Ag solder material degraded the elastic properties which can negatively impact on the life-time of electronic devices.

4 Conclusions

The present work investigates the thermal aging impacts on structure, electrical resistivity, elastic moduli and damping characteristic of a lead-free Sn–3.5Ag material. From micro-structure analysis, the fine network-type Ag_3Sn IMC phase and bamboo-like β-Sn grains in certain direction were found in as-cast solder material. However, after isothermal aging the remarkable changes in the microstructure were observed in presence of Sn grain size, grain orientation, cyclic twin with a special orientation <100> 60° relationship with the matrix grains and IMC growth which impacts on the material properties of Sn–3.5Ag material. The damping property of Sn–3.5Ag material enhanced after exposing at harsh environments. Consequently, the elastic/shear moduli as well as electrical resistivity of Sn–3.5Ag material were significantly degraded. A comparison between as-cast solder material and aged solder material presents that the reductions in shear and elastic moduli were approximately 39% and 23.3, respectively, where as in electrical resistivity degradation was approximately 12.8%. The material properties degradation

behavior of electronic interconnect material can minimize the life-time of modern green electronics.

References

1. K. Lee, K.S. Kim, Y. Tsukada, K. Suganuma, K. Yamanaka, S. Kuritani, M. Ueshima, Microelectron. Reliab. **51**, 2290 (2011)
2. A.A. El-Daly, T.A. Elmosalami, W.M. Desoky, M.G. El-Shaarawy, A.M. Abdraboh, Mater. Sci. Eng. A **618**, 389 (2014)
3. A.K. Gain, L. Zhang, J. Mater. Sci. **27**, 781 (2016)
4. M.M. A.S.M.A. Haseeb, S.L. Arafat, Y.M. Tay, Leong, J. Electron. Mater. **46**, 5503 (2017)
5. A.K. Gain, L. Zhang, J. Mater. Sci. **28**, 9363 (2017)
6. H.R. Kotadia, P.D. Howes, S.H. Mannan, Microelectron. Reliab. **54**, 1253 (2014)
7. A.K. Gain, L. Zhang, J. Mater. Sci. **28**, 4885 (2017)
8. Y. Plevachuk, W. Hoyer, I. Kaban, M. Kohler, R. Novakovic, J. Mater. Sci. **45**, 2051 (2010)
9. A.K. Gain, Y.C. Chan, A. Sharif, W.K.C. Yung, Microelectron. Eng. **86**(11), 2347 (2009)
10. F. Gnecco, E. Ricci, S. Amore, D. Giuranno, G. Borzone, G. Zanicchi, R. Novakovic, Int. J. Adhes. Adhes. **27**, 409 (2007)
11. A.K. Gain, T. Fouzder, Y.C. Chan, A. Sharif, N.B. Wong, W.K.C. Yung, J. Alloys Compd. **506**, 216 (2010)
12. A.K. Gain, T. Fouzder, Y.C. Chan, A. Sharif, W.K.C. Yung, J. Alloys Compd. **489**(2), 678 (2010)
13. A.K. Gain, L. Zhang, Y.C. Chan, J. Mater. Sci. **26**(9), 7039 (2015)
14. J.W. Yoon, J.H. Bang, C.W. Lee, S.B. Jung, J. Alloys Compd. **627**, 276 (2015)
15. A.K. Gain, L. Zhang, Microelectron. Reliab. **83**, 101 (2018)
16. M. Pourmajidian, R. Mahmudi, A.R. Geranmayeh, S. Hashemizadeh, S. Gorgannejad, J. Electron. Mater. **45**, 764 (2016)

17. Y. Wang, J. Han, L. Ma, Y. Zuo, F. Guo, J. Electron. Mater. **45**, 6095 (2016)
18. M. Sahin, E. Cadirli, J. Mater. Sci.: Mater. Electron. **23**, 484 (2012)
19. N. Chawla, Int. Mater. Rev. **54**(6), 368 (2009)
20. A.K. Gain, L. Zhang, J. Mater. Sci. **27**(7), 7524 (2016)
21. A.K. Gain, L. Zhang, J. Mater. Sci. **27**, 3982 (2016)
22. D.S. Steinberg, *Vibration Analysis for Electronic Equipment*, Second edn. (Wiley, New York, 1998)
23. A.K. Gain, L. Zhang, J. Alloys Compd. **617**, 779 (2014)
24. S.H. Chang, S.K. Wu, Scripta Mater. **63**, 957 (2010)
25. A.K. Gain, L. Zhang, J. Mater. Sci. **27**, 11273 (2016)
26. S.H. Chang, S.K. Wu, Scripta Mater. **64**, 757 (2011)
27. E.H. Wong, S.K.W. Seah, V.P.W. Shim, Microelectron. Reliab. **48**, 1747 (2008)
28. X. Hu, Y. Li, Z. Min, J. Alloys Compd. **582**, 341 (2014)
29. G. Zeng, S.D. McDonald, D. Mu, Y. Terada, H. Yasuda, Q. Gu, M.A.A. Mohd Salleh, K. Nogita, J. Alloys Compd. **685**, 471 (2016)
30. A.K. Gain, L. Zhang, M.Z. Quadir, Mater. Des. **110**, 275 (2016)
31. A.K. Gain, L. Zhang, M.Z. Quadir, Mater. Sci. Eng. A **662**, 258 (2016)
32. T. Laurila, V. Vuorinen, J.K. Kivilahti, Mater. Sci. Eng. R **49**(1–2), 1 (2005)
33. S.K. Kang, W.K. Choi, D.Y. Shih, D.W. Henderson, T. Gosselin, A. Sarkhel, C. Goldsmith, K.J. Puttlitz, JOM **55**(6), 61 (2003)
34. D.W. Henderson, T. Gosselin, A. Sarkhel, S.K. Kang, W.K. Choi, D.Y. Shih, C. Goldsmith, K.J. Puttlitz, J. Mater. Res. **17**(11), 2775 (2002)
35. S.K. Seo, S.K. Kang, D.Y. Shih, H.M. Lee, J. Electron. Mater. **38**(2), 257 (2009)
36. A.U. Telang, T.R. Bieler, J.P. Lucas, K.N. Subramanian, L.P. Lehman, Y. Xing, E.J. Cotts, J. Electron. Mater. **33**(12), 1412 (2004)
37. I.E. Anderson, J.C. Foley, B.A. Cook, J. Harringa, R.L. Terpstra, O. Unal, J. Electron. Mater. **30**, 1050 (2001)
38. K.D. Kim, D.D.L. Chung, J. Electron. Mater. **31**(9), 933 (2002)
39. P. Babaghorbani, S.M.L. Nai, M. Gupta, J. Alloys Compd. **478**, 458 (2009)
40. S.K. Wu, S.H. Chang, W.L. Tsia, H.Y. Bor, Mater. Sci. Eng. A **528**, 6020 (2011)
41. A.V. Granato, K. Lucke, J. Appl. Phys. **52**, 7136 (1981)
42. Z. Trojanova, W. Riehemann, H. Ferkel, P. Lukac, J. Alloys Compd. **310**(1–2), 396 (2000)